JACS
JOURNAL OF THE AMERICAN CHEMICAL SOCIETY
Article
pubs.acs.org/JACS

Super-Reduced Polyoxometalates: Excellent Molecular Cluster Battery Components and Semipermeable Molecular Capacitors

Yoshio Nishimoto,[†] Daisuke Yokogawa,[†,‡] Hirofumi Yoshikawa,[†,§] Kunio Awaga,[†,§] and Stephan Irle*[,†,‡]

[†]Department of Chemistry, Graduate School of Science, Nagoya University, Nagoya 464-8602, Japan
[‡]Institute of Transformative Bio-Molecules (WPI-ITbM), Nagoya University, Nagoya 464-8602, Japan
[§]Research Center for Materials Science, Nagoya University, Nagoya 464-8602, Japan

Supporting Information

ABSTRACT: Theoretical investigations are presented on the molecular and electronic structure changes that occur as α-Keggin-type polyoxometalate (POM^{3-}) clusters $[PM_{12}O_{40}]^{3-}$ (M = Mo, W) are converted toward their super-reduced POM^{27-} state during the discharging process in lithium-based molecular cluster batteries. Density functional theory was employed in geometry optimization, and first-principles molecular dynamics simulations were used to explore local minima on the potential energy surface of neutral POM clusters adorned with randomly placed Li atoms as electron donors around the cluster surface. On the basis of structural, electron density, and molecular orbital studies, we present evidence that the super-reduction is accompanied by metal−metal bond formation, beginning from the 12th to 14th excess electron transferred to the cluster. Afterward, the number of metal−metal bonds increases nearly linearly with the number of additionally transferred excess electrons. In α-Keggin-type POMs, metal triangles are a prominently emerging structural feature. The origin of the metal triangle formation during super-reduction stems from the formation of characteristic three-center two-electron bonds in triangular metal atom sites, created under preservation of the POM skeleton via "squeezing out" of oxygen atoms bridging two metal atoms when the underlying metal atoms form covalent bonds. The driving force for this unusual geometrical and electronic structure change is a local Jahn−Teller distortion at individual transition-metal octahedral sites, where the triply degenerate t_2 d orbitals become partially filled during reduction and gain energy by distortion of the octahedron in such a way that metal−metal bonds are formed. The bonding orbitals show strong contributions from mixing with metal−oxygen antibonding orbitals, thereby "shuffling away" excess electrons from the cluster center to the outside of the cage. The high density of negatively charged yet largely separated oxygen atoms on the surface of the super-reduced POM^{27-} polyanion allows the huge Coulombic repulsion due to the presence of the excess electrons to be counterbalanced by the presence of Li countercations, which partially penetrate into the outer oxygen shell. This "semiporous molecular capacitor" structure is likely the reason for the effective electron uptake in POMs.

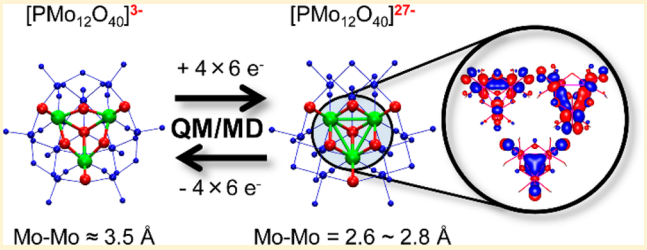

INTRODUCTION

Polyoxometalate (POM) was first reported by Jöns Jacob Berzelius in 1826,[1,2] and it was later found that this substance contains the $[PMo_{12}O_{40}]^{3-}$ anion. However, its precise molecular structure remained unknown for more than 100 years, until James F. Keggin resolved the structure of a related heteropolyacid species, $H_3[PW_{12}O_{40}]\cdot nH_2O$, using X-ray spectroscopy in 1933.[3] His data indicated that a central PO_4^{3-} tetrahedral group is surrounded by 12 fused WO_6 octahedrons sharing oxygens at their edges or vertices and that the trianion adopts T_d symmetry. It later was confirmed that virtually all $[XM_{12}O_{40}]^{x-}$-type POMs (X = P, Si, Al, etc.; M = Mo, W, V, etc.) feature this so-called α-Keggin structure. Other relevant POM structures, for instance, the smaller homopoly Lindqvist structure[4] ($[M_6O_{19}]^{2-}$) and larger heteropoly structures such as the Anderson−Evans[5,6] ($[XM_6O_{24}]^{x-}$) and Dawson[7] ($[X_2M_{18}O_{62}]^{x-}$) structures, have been reported as well. With only a few exceptions, almost all chemical elements have been either incorporated into POM structures themselves or encapsulated within them.[8]

In recent years, the number of experimental[9−12] as well as theoretical[13−18] investigations of various POM clusters has increased because of their fascinating molecular and electronic structures and properties. However, the presence of a minimum of six transition-metal atoms in even the smallest possible POM anions represents a challenge for substantive quantum-chemical studies.[8] Fortunately, in recent years, reasonably accurate density functional theory (DFT) has become applicable to such large and complicated molecular systems. Thus, thanks to combined experimental and theoretical efforts, a variety of POM properties such as catalytic activity,[9,10,16] single-molecule magnetism,[11] and electrochemical redox potentials[12,18−20] are now fairly well understood.

Received: April 1, 2014
Published: June 2, 2014

dx.doi.org/10.1021/ja5032369 | J. Am. Chem. Soc. 2014, 136, 9042−9052

One of the most intriguing properties of POM clusters is their highly unusual capability to accept a large number of electrons,[21−24] a property that finds its expression in the terms "electron reservoir"[2] or "electron sponge"[25] sometimes used in the literature. This means for instance that POM clusters have the potential to play an important role as a cathode-active material. In the mid-1970s, Jean Pierre Launay[24] reported the preparation and characterization of electrochemically highly reduced metatungstate anions.[2] On the basis of the observation of irreversible electrode reactions and simple molecular orbital (MO) considerations, he and his co-workers proposed that *three* joint octahedra constituting each of the four corners of the POM cluster would be reduced by up to six electrons and that *this locally reduced structure would feature* W^{IV}−W^{IV} *bonds arranged in the form of triangles.*[24] However, these suggestions were mere speculation and lacked any direct evidence. More recently, our team reported that in high-capacity lithium batteries[23,25−27] a Keggin POM anion containing 12 Mo atoms may indeed hold 24 excess electrons, as determined by in situ-observed changes in the Mo ion average valences derived from Mo K-edge absorption edge energies of X-ray absorption near-edge structure (XANES) data.[25] This high uptake of excess electrons (termed "super-reduction" in ref 25) is the current confirmed record for a single molecular cluster and is certainly remarkable since highly charged anions are usually prone to break covalent bonds and decompose spontaneously. Other chemical compounds exhibiting the features of super-reduction are Mn_x[26,27] and iron−sulfur[28,29] clusters, although these compounds can accommodate only up to eight and four excess electrons per cluster, respectively. Thus, to achieve super-reduction, it is necessary to use molecular clusters with a large number of transition-metal atoms. Since POMs are famous for their capability to form supramolecular condensates with well-defined structures,[2] they possess tremendous potential for the design of molecular clusters capable of super-reduction, possibly even exceeding the current record of 24-electron super-reduction.

In the present work, we focus on the question of how the Keggin-type POM cluster can reach a super-reduced state in a molecular cluster battery (MCB) without being ripped apart by the repulsive Coulombic forces due to the large number of excess electrons. In the extended X-ray absorption fine structure (EXAFS) spectrum reported by Wang et al.,[25] three unique structural changes were reported during reduction by up to 24 electrons: (i) most notably, the overall Mo−Mo distances shrank from about 3.6 Å in the "native" Keggin $[PMo_{12}O_{40}]^{3-}$ cluster trianion[30] to about 2.6 Å; (ii) the Mo−O bonds pointing outward away from the cluster [the Mo−O (out) bonds; see Figure 1] increased in length from 1.7 to about 1.9 Å; and (iii) the inner Mo−O [Mo−O (in)] bonds were shortened from 2.4 to about 2.0 Å.

To better understand these structural changes recorded in situ by EXAFS, we performed our study theoretically by means of DFT calculations using both static and first-principles molecular dynamics (FPMD) approaches. For the discussion of changes in molecular and electronic state structure during reduction, we combined available experimental and theoretical data and employed MO analyses in combination with ligand field theory.[31] Our approach models the super-reduced state of POM by supplying explicit alkali-metal atoms around the POM cluster in the DFT calculations.

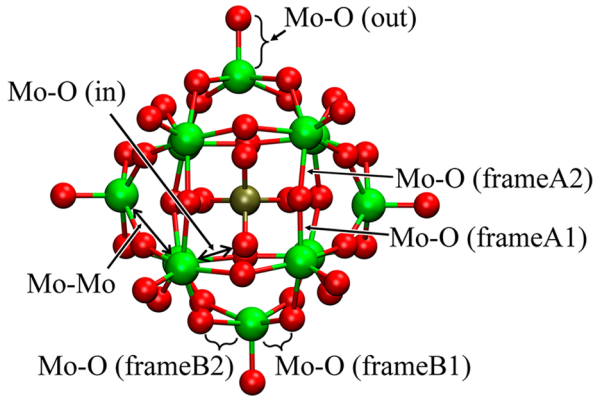

Figure 1. BP86-D-optimized structure of $[PMo_{12}O_{40}]^{3-}$ and definitions of characteristic bond lengths. The green-, red-, and olive-colored spheres represent molybdenum, oxygen, and phosphorus atoms, respectively.

COMPUTATIONAL DETAILS

The present study mainly employed the heteropolymolybdate α-Keggin polyoxometalate cluster $[XMo_{12}O_{40}]^{3-}$ (X = P) as the model system, and we refer to this particular Keggin cage as "POM" in the remainder of the paper. Several calculations were also carried out for its tungsten analogue $[XW_{12}O_{40}]^{3-}$ (X = P), and in these cases we refer to the Keggin cage as "W-POM". All of the molecular and electronic structure calculations as well as the on-the-fly direct FPMD simulations were carried out using DFT[32,33] as implemented in the TURBOMOLE code.[34] We selected the BP86 exchange−correlation[35,36] and B3LYP[37] hybrid functionals with the all-electron, polarized split-valence-type def-SV(P) basis set[38] [hereafter abbreviated as SV(P)] for Li, O, Na, and P atoms and the TURBOMOLE standard effective core potentials (ECPs) for Mo and W.[39] The semiempirical dispersion correction as formulated by Grimme[40] was introduced in order to describe long-range van der Waals interactions, and the functionals with this correction are denoted with a "-D" suffix. A geometry optimization using a larger valence triple-ζ-quality basis set (TZVPP)[41] for all elements was also performed for the "native" POM^{3-} cluster. For all of the BP86 DFT calculations, we introduced the resolution of identity (RI) approximation[42] in combination with optimized auxiliary basis sets,[38,39,41,43] which significantly enhanced the speed of calculation with negligible loss of accuracy. No symmetry constraints were applied in the calculations if not explicitly mentioned otherwise. In all of the calculations we assumed a closed-shell singlet state and used spin-restricted MOs. For a few selected cases, we computed energies of electronic states with higher spin multiplicities and found that they were usually higher than singlet energies, indicating that the system tries to adopt a low spin electronic ground state whenever possible.

The calculations on the POM^{3-} cluster were carried out in the absence of explicit counterions (i.e., assuming three negative charges on this cluster) unless indicated otherwise. In order to model the reduced $POM^{(3+n)-}$ clusters, we added 3 + *n* neutral alkali-metal atoms (either lithium or sodium) around a neutral POM cluster and set the total charge of the system in the DFT calculation to zero. For the FPMD simulations in the canonical *NVT* ensemble, the environmental target temperature was controlled by the Nose−Hoover chain thermostat[44−46] as implemented in the TURBOMOLE code (program "frog") The target temperature was set to 500 K. The thermostat relaxation time was 12.094 fs and the time integration interval was 1.935 fs, since no light hydrogen atoms are included in the system.

For MO-based population analyses, we employed the AOMix[47,48] code, and analysis of the charge densities was carried out on the basis of natural population analysis (NPA)[49] as well as Wiberg bond orders.[50] For visualization of molecular and electronic structures, the VMD[51] and gOpenMol[52,53] software packages were used.

dx.doi.org/10.1021/ja5032369 | J. Am. Chem. Soc. 2014, 136, 9042−9052

RESULTS AND DISCUSSION

Molecular Structure of the Native Keggin POM^{3-}. The initial geometry of the heteropolymolybdate POM^{3-} (X = P) cluster was taken from the X-ray structure of Liu et al.[30] We subjected this geometry to structural optimization at the BP86-D/SV(P) and B3LYP-D/SV(P) levels of theory in vacuum without explicit counterions, assuming a total charge of −3. Table 1 displays key structural parameters for the crystal structure and the BP86-D- and B3LYP-D-optimized geometries along with root-mean-square deviations (RMSDs) of the theoretical geometries from the crystal structure. Although experimentally the metal−oxygen bond lengths for α-Keggin POMs are typically divided into three categories, we identified different types, consistent with a previous theoretical study by the Poblet group,[17] namely Mo−O (out), Mo−O (in), Mo−O (frameA1), Mo−O (frameA2), Mo−O (frameB1), and Mo−O (frameB2). In T_d symmetry, Mo−O (frameA1) is identical to Mo−O (frameA2) and Mo−O (frameB1) is identical to Mo−O (frameB2), but these pairs are in fact nonequivalent in lower-symmetry calculations, as will be discussed below. The Cartesian coordinates after the geometry optimizations are given in the Supporting Information (SI) and are labeled as structure **1** (BP86-D) and structure **2** (B3LYP-D) for POM and structure **3** (BP86-D) for W-POM. The RMSD of the Cartesian coordinates was defined as usual without mass weighting and measures structural deviations between maximally overlapping structures. It can be seen that the DFT bond lengths do not deviate from the X-ray structure by more than 0.1 Å. The largest deviation can be seen for the Mo−O (frame) bond lengths.

Table 1. Comparison of Key Structural Parameters in the X-ray[30] and DFT-Optimized Structures of POM^{3-} [a]

	X-ray	BP86-D	B3LYP-D
Mo−Mo	3.563	3.606	3.609
Mo−O (out)	1.684	1.719	1.703
Mo−O (in)	2.442	2.452	2.461
Mo−O (frameA1)	1.920	1.882	1.855
Mo−O (frameA2)		2.011	2.031
Mo−O (frameB1)	1.915	1.867	1.843
Mo−O (frameB2)		1.995	2.016
RMSD[b]	0.000	0.127	0.152

[a]All values are given in units of Å. The locations of the bond types are given in Figure 1. [b]RMSD values of BP86-D and B3LYP-D are calculated with respect to the X-ray structure as reference.

The existence of different Mo−O (frame) bond lengths in POMs was reported previously in the theoretical study by Yan et al.[17] They observed alternating bond length (ABL) distortions and found that the origin of these distortions, which lower the point-group symmetry from T_d to chiral T, is a pseudo-Jahn−Teller vibronic instability. In Table 1, the ABL distortions are clearly visible in our computed geometries, obtained by geometry optimizations without symmetry restrictions. The averages over these four Mo−O types are 1.939 and 1.936 Å using BP86-D and B3LYP-D, respectively, in good agreement with the X-ray structure. In fact, the BP86-D- and B3LYP-D-optimized geometries are remarkably similar, even though B3LYP itself is typically more suitable for systems containing main-group elements.[54] Indeed, the RMSD values indicate that the BP86-D structure is in slightly better agreement with the X-ray data than the B3LYP-D structure, confirming a general trend in the performance of various DFT functionals for transition-metal-containing systems.[55] We additionally performed a BP86-D calculation with a larger basis set (TZVPP) to validate our general use of the double-ζ-quality SV(P) basis set. The geometry was similar to the SV(P)-optimized result, and the corresponding RMSD value of this structure with respect to the X-ray geometry was 0.134 Å, indicating that our results did not have significant basis set dependence in the prediction of geometries. Overall, the trend of DFT gas-phase optimizations toward larger cage structures is indicative of the important role of crystal field effects on POM^{3-} molecular cluster geometries. On the basis of these results, we therefore decided to employ the BP86-D method for the study of POM redox processes because of its reasonable performance and low computational cost.

Strategies for Modeling the Molecular and Electronic Structures of Reduced POMs. The quantum-chemical study of anions is notoriously difficult, and to make matters worse, even though multiply charged anions, such as SO_4^{2-}, CO_3^{2-}, and PO_4^{3-}, are ubiquitous in chemistry, they are not stable with respect to autodetachment as isolated species in the gas phase.[56] Clearly, to accurately describe polyanionic species theoretically, it would be required to (a) accurately account for electron correlation, (b) use sufficiently large basis sets to accommodate the diffuse electron density of negatively charged species, and (c) include the environment of the molecular polyanion in the quantum-chemical calculation. Presently none of the available quantum-chemical methodologies are capable of "precisely" taking into account any of these three important theoretical requirements, let alone all three of them together. Thus, any attempt to model a super-reduced POM molecular cluster has to be conducted within the current limits of computational feasibility, and solid experimental observations must be used to compensate for methodological deficiencies.

Since the Keggin POM contains 12 transition-metal atoms plus 40 oxygen atoms, ab initio methods such as second-order Møller−Plesset perturbation theory[57] or configuration interaction[58] are out of the question for the treatment of electron correlation effects. DFT is presently the only computationally feasible method here, and we have to accept its predictions without a thorough check by more accurate methods and with only limited complementary information from EXAFS spectra. In terms of the basis set, as we have already indicated above, the split-valence polarized basis set plus ECPs for the transition metals is sufficiently accurate to describe the geometry of the POM^{3-} cluster. Since our approach of modeling the super-reduced state involves the calculation of charge-neutral species by way of inclusion of explicit counterions, the use of larger basis sets is not expected to qualitatively change the BP86-D/SV(P) results of our investigations, in particular since the large number of diffuse basis functions from the alkali-metal atoms provides additional flexibility in the description of the MOs of the super-reduced POMs.

Finally, the atomistic structure of the POM cluster environment in the MCB during charging and discharging is presently unknown, and we thus relied on the assumption that close contacts between the reduced POMs and the countercations (Li^+) and the dielectric field of the graphitic solid, surrounded by the ethylene carbonate solvent, stabilize the super-reduced species.[25] The influence of the countercations is dominant among the interactions with the cluster environment, and for this reason we explicitly included them in all calculations on super-reduced POMs. However, estimates of

dx.doi.org/10.1021/ja5032369 | J. Am. Chem. Soc. 2014, 136, 9042−9052

their number and positions are not available from experiment, and it can be expected that in MCBs large ion density fluctuations can easily occur. Our approach for adding Li^+ or Na^+ counterions in the DFT calculations therefore followed a somewhat heuristic approach. We note in passing that Fleming et al.[59] theoretically investigated the effect of absorption of a cluster anion onto a gold surface using polarization-induced mirror charges, but the explicit use of alkali-metal counterions is more accurate for modeling of a Li-ion battery component than a mirror charge model. Since no detailed structural information for solid and liquid environmental compounds is available from the experiment, we chose to neglect their influence entirely.

Geometry Optimizations of Super-Reduced POMs. At first we attempted to perform calculations with 27 Li atoms surrounding a neutral POM cluster starting from the X-ray structure of the POM^{3-} Keggin trianion.[30] The Li atoms were initially positioned randomly around the cage, sufficiently close for interaction. After a full geometry optimization of this system, we obtained the structure shown in Figure 2 (labeled as structure **4** in the SI). We noticed a substantial rearrangement of the positions of the Li atoms during the relaxation of the structure. The final POM structure contained four significantly shortened Mo−Mo distances (less than 3.0 Å), three of which formed a triangular Mo site consisting of Mo−Mo bonds in the range from 2.65 to 2.77 Å with an average of 2.73 Å (see Figure 2A). These bond lengths are only slightly longer than the previously reported experimental bond length of 2.6 Å for the super-reduced POM from EXAFS,[25] and they confirm that super-reduction induces Mo−Mo bond formation. In addition, we found that Mo−O (out) bonds for Mo atoms involved in Mo−Mo bonding had significantly stretched by ∼0.2 Å to 1.97 Å on average, while the Mo−O (in) bonds were compressed by a similar amount to 2.18−2.20 Å (see Figure 2B). These changes in Mo−O bond distances are also in agreement with experimental findings. The ABL related to Mo−O (frame1) and Mo−O (frame2) bonds vanished, and the Mo−O (frame) bonds in this geometry exhibited values between 2.13 and 2.23 Å. This makes the Mo−O (frame) bonds difficult to distinguish from significantly shortened Mo−O (in) bonds in the super-reduced species.

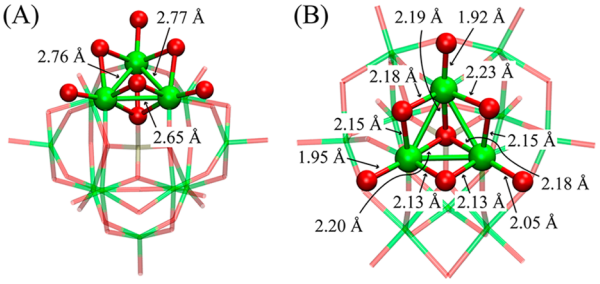

Figure 2. Optimized structure of POM with 27 Li, labeled as structure **4** in the SI: (A) side view showing Mo−Mo distances; (B) top view of the triangular Mo site showing Mo−O (in), Mo−O (out), and Mo−O (frame) distances. Alkali-metal atoms have been omitted for clarity. See Figure 1 for the definition of colors.

NPA[49] carried out on this ad hoc optimized POM + 27 Li structure **4** indicated that the POM cluster had taken up only 21.2 electrons from the Li atoms, as estimated from the NPA point charge distribution. We performed similar calculations with modified initial geometries of Li atoms and obtained varying structures, sometimes with and sometimes without Mo triangles. The corresponding total energies of these POM + 27 Li isomers varied on a hundred kcal/mol energy scale as a result of the strong Coulombic interactions between the counter-cations and the negatively charged POM cluster. These explorative studies demonstrated that the potential energy surface (PES) of the POM + 27 Li system is very rough, featuring high barriers separating minimum-energy structures associated with Li migration and POM structural changes.

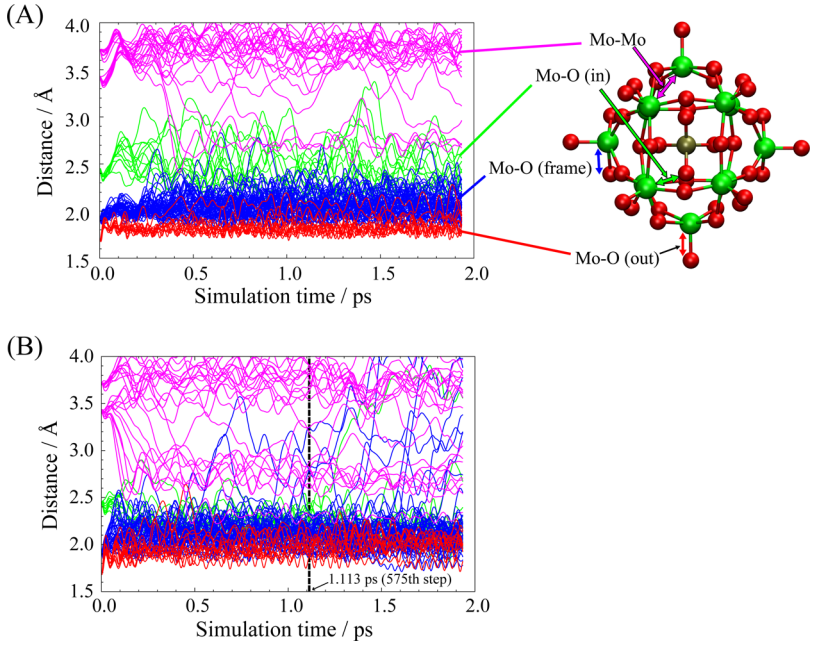

Figure 3. Histograms of the bond-length fluctuations during the MD simulations of the POM cluster with (A) 27 and (B) 35 explicit Li atoms. As illustrated in the structure at the right, the bond types are color-coded as follows: Mo−Mo, pink; Mo−O (out), red; Mo−O (in), green; Mo−O (frame), blue. The vertical dotted line in (B) indicates the snapshot geometry at 1.113 ps that we selected for subsequent geometry optimization of the POM + 35 Li system.

dx.doi.org/10.1021/ja5032369 | J. Am. Chem. Soc. 2014, 136, 9042−9052

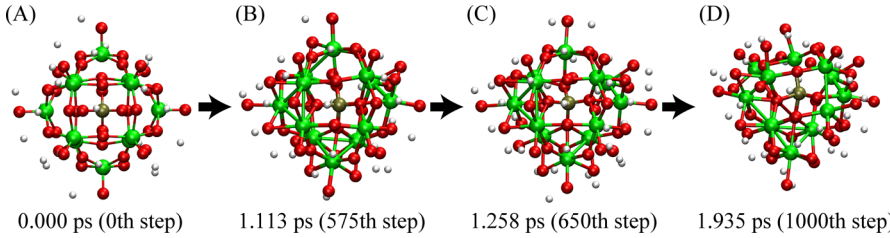

Figure 4. Selected snapshots from trajectory B at (A) 0.000 ps (the initial structure), (B) 1.113 ps, (C) 1.258 ps, and (D) 1.935 ps (at the end of the MD simulation). See Figure 1 for the definition of P, O, and Mo colors; white spheres represent Li atoms.

Clearly, ad hoc geometry optimizations became trapped in local minima that were structurally related to the initial choice of Li atom placement. In order to investigate the PES more broadly and avoid entrapment close to the initial geometries, we decided to perform on-the-fly FPMD simulations with subsequent structure optimization ("quenching") on the basis of BP86-D/SV(P) energies and gradients.

Molecular Dynamics Simulations of Super-Reduced POMs. We adopted a relatively high temperature of 500 K for the FPMD simulations in order to more fully explore the associated PES. We note that although the MCB experiments had been carried out at room temperature,[25] the local temperature close to the POM clusters might actually be closer to the target temperature of our MD simulation.

At first, we subjected the previously described POM + 27 Li system to FPMD simulations starting from the POM^{3-} X-ray geometry (trajectory A). Figure 3A displays structural changes during the entire length of the MD simulation traced by the bond lengths for Mo−Mo in pink, Mo−O (out) in red, Mo−O (in) in green, and Mo−O (frame) in blue. The FPMD simulation was performed for 1000 time integration steps (i.e., for a total of 1.935 ps). The bond lengths undergo dramatic changes, in particular during the first 0.5 ps, indicating that major structural changes in the cage induced by electron transfer from Li atoms to the POM cluster take place during this time period. Most notably, three to four short Mo−Mo distances around 2.5−2.8 Å quickly appear in this FPMD simulation, starting at around 0.39 ps. When a bond is formed between two Mo centers, it follows that their distances to other Mo centers must increase, and therefore, a large variation in Mo−Mo distances can be observed. The Mo−O (out) bonds significantly stretch immediately from 1.7 Å (characteristic of the optimized POM^{3-} structure) to an average of 1.85 Å in the FPMD simulations. The Mo−O (in) and Mo−O (frame) bond lengths fluctuate with larger amplitudes around average values of 2.47 and 2.06 Å, respectively, indicating that the structural integrity of the POM cluster is compromised. The averages and amplitudes of these particular bond-length fluctuations appear to be converged after around 1 ps of simulation time.

We then proceeded to perform a geometry optimization of the final trajectory snapshot at 1.935 ps, which resulted in a structure that features three short Mo−Mo bonds (<3.0 Å) with bond lengths of around 2.68−2.69 Å, creating one Mo triangle (listed as structure **5** in the SI). The NPA of the charge distribution in this POM + 27 Li cluster shows that 22.7 electrons were transferred to the POM, indicating once again that the charge transfer from Li is only partial in nature, at least within the limitations of an atomic point charge analysis. Replacing the 27 Li atoms with more electropositive Na atoms resulted in the counterintuitive result of reduced charge transfer to the POM. This simulation, the resulting POM + 27 Na structure **6**, and the origin of the ineffectiveness of the larger sodium atoms[60] in reducing the POM cluster are discussed in the SI. We note that such a counterintuitive result also has been reported for instance in the difference of the solvent stabilization potentials of small, polar water molecules and larger, purely ionic liquid cations.[61]

To summarize, the simulations we had performed thus far hinted at a qualitative relationship between the number of excess electrons on the POM and the appearance of short Mo−Mo bonds. Since Li was apparently more effective in achieving POM reduction, we decided to add up to eight more Li atoms to the POM + 27 Li system. Geometry optimizations starting from the initial structure **5** after the addition of eight more Li atoms at random initial positions around the cluster resulted in a structure that featured a total of six short Mo−Mo bonds, one complete and one partial triangular Mo site, and one Mo−Mo single bond with a Wiberg bond order[50] of 0.936 (structure **7** in the SI). We then proceeded with FPMD simulations of the POM + 35 Li system following the same "recipe" as described above (i.e., starting from the POM^{3-} X-ray geometry and randomly supplying 35 Li atoms around this cluster). As before, we employed a target temperature of 500 K and performed the simulation for 1.935 ps, generating trajectory B. Figure 4 displays selected snapshot geometries representing the structural changes occurring in this trajectory. In this case, we observed that during the FPMD simulation the POM + 35 Li cluster gradually disintegrated after around 1.26 ps, as can be seen in the rotated view of the final geometry in Figure 4D, which shows completely dissociated oxygen bound to nearby Li. The tendency toward disintegration can also be seen in the time evolution of the Mo−O (frame) bond lengths in Figure 3B, which start to exceed distances of around 3.0 Å starting from 1.2 ps.

Figure 5 displays the RMSD of the POM cluster atomic coordinates in trajectory B, except for Li atoms, with respect to the initial geometry (the POM^{3-} X-ray geometry). At first, the RMSD value steeply increases as a sign of changes in the POM molecular structure and then relatively quickly stabilizes at around 0.5 Å up to 1.3 ps, just after the snapshot in Figure 4C. Afterward, gradual disintegration of the cluster is shown by a continuous increase in the RMSD. We conclude that it is difficult to accommodate 35 Li atoms around the Keggin POM cluster, at least at the high temperature of our MD simulation.

For further geometry analysis, in this case we extracted a snapshot geometry before cage disintegration, namely, the structure at 1.113 ps (see Figure 4B, corresponding to the structure at the vertical dotted line in Figure 3B), and subjected it to geometry optimization. The resulting POM + 35 Li molecular structure (structure **8** in the SI) featured *two* triangular Mo sites, two single Mo−Mo bonds, and even one Mo═Mo double bond. The NPA indicates a charge transfer of

dx.doi.org/10.1021/ja5032369 | J. Am. Chem. Soc. 2014, 136, 9042−9052

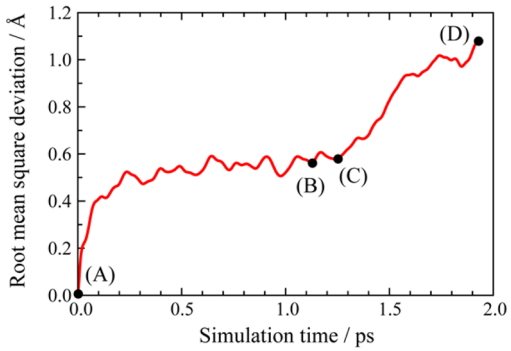

Figure 5. RMSD of the POM cluster with respect to the POM^{3-} X-ray geometry during trajectory B as a function of the simulation time. The labels in the plot identify the snapshots displayed in Figure 4

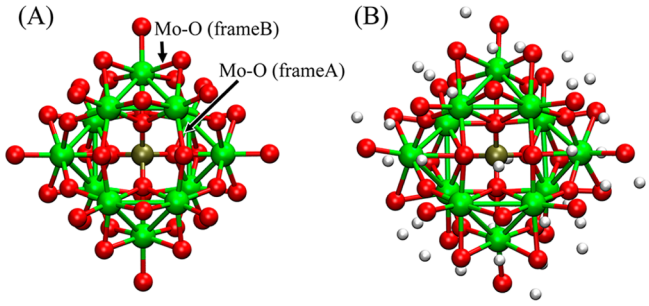

Figure 6. (A) Constructed structure containing four triangular Mo sites and (B) its optimized structure with 35 Li atoms. The Mo−Mo bond threshold is 3.0 Å. See Figure 1 for the definition of colors; the white spheres represent Li atoms.

28.3 electrons from Li to the POM. The bond orders were estimated by Wiberg bond order analysis,[50] which gave Mo−Mo bond order sums of 2.32 and 2.51 for the two triangular Mo sites, 0.97 and 1.15 for the Mo−Mo single bonds, and 2.20 for the Mo═Mo double bond, consistent with a very short distance of only 2.33 Å. Similar results were obtained for the W-POM + 35 Li system, only here the number of W−W bonds was typically smaller, with about one metal triangle plus an addition metal−metal bond. The POM + 35 Li structure **8** obtained by MD quenching is substantially more stable than the initially optimized structure **7** by 2.95 eV (67.9 kcal/mol), although it is difficult to clarify whether this difference originates from the difference in the number of Mo triangles and Mo−Mo interactions or from the difference in the positions of Li atoms.

Four Metal Atom Triangles in Super-Reduced Keggin POMs. The quenched POM + 35 Li structure **8** from trajectory B was the lowest-energy structure we could identify thus far and had the largest numbers of Mo−Mo bonds (eight single bonds and one double bond) and Mo triangles (two). However, the reported experimental structural data support the notion that *all* of the Mo−Mo distances in super-reduced POM are converted to short (<3.0 Å) Mo−Mo single bonds, suggesting that each Keggin cage contains four triangular Mo sites.[25] One possible reason for this discrepancy is that despite the relatively high temperature of 500 K, the MD simulation became still entrapped in a local minimum.

In order to theoretically investigate the hypothesis of a super-reduced POM cage with the maximum number of four Mo triangles, we "constructed" a super-reduced POM geometry in T_d symmetry by combining four subunits of three octahedrons to create four Mo−Mo triangles, similar to the structure proposed by Launay[24] and others.[2] In this "constructed" structure (structure **9** in the SI, shown in Figure 6A), all of the Mo−O (out) distances were set to 1.90 Å and the Mo−O (frame) and Mo−O (in) distances were set to 2.00 Å following the experimental observations,[25] while the Mo−Mo distances were assumed to be 2.65 Å on the basis of our previous geometry optimizations of super-reduced POM models. After adorning this cluster with 35 Li atoms at random positions around this constructed structure, we performed a geometry optimization without symmetry constraints. As a result, we obtained a less symmetric cluster (structure **10** in the SI, shown in Figure 6B) that however featured the maximum number of four triangular units with 12 Mo−Mo bonds in the range from 2.61 to 2.84 Å, indicating the existence of such a minimum-energy structure with the maximum number of Mo−Mo triangles. The Mo−O (in) and Mo−O (out) bonds were optimized to values ranging from 2.06 to 2.15 Å and from 1.93 to 2.15 Å, respectively. We note that the Mo−O (frame) bonds are now split into two groups, termed Mo−O (frameA) and Mo−O (frameB), with similar bond lengths ranging from 2.0 to 2.1 Å. However, while the distance of O (frameA) atoms from the central phosphorus atom (about 3.2 Å) does not change significantly during super-reduction, the O (frameB) atoms are "squeezed out" of the cage as a result of the formation of the underlying Mo−Mo bond, and their distance to the P atom is greatly elongated by up to 4.7 Å during the reduction. Consequently, the Mo−O (frameA)−Mo and Mo−O (frameB)−Mo angles are very different, with values of around 133° and 77°, respectively. Thus, the structural change in the POM cage during super-reduction causes a greater presence of oxygen atoms on its outer surface.

The "constructed" and subsequently optimized POM + 35 Li structure **10** agrees well with our previously reported EXAFS data. NPA shows that the cluster has 28.3 excess electrons. Its energy is 1.44 eV (33.2 kcal/mol) higher than that of the quenched POM + 35 Li structure **8**, which may be due to an unfavorable arrangement of the Li atoms in the initial geometry. A similarly constructed and optimized structure of the W-POM cluster is given in the SI as structure **11**, and the frontier MO patterns for the W analogue of the previously described Mo-based POM^{27-} super-reduced cluster are identical. Thus, we conclude that the occurrence of metal triangles during super-reduction of Keggin POM clusters is not limited to only heteropolyoxomolybdate but also applies to W-POM.

MO Analysis of POM Super-Reduction. For the detailed electronic structure analysis of the super-reduced species, we did not explicitly include alkali-metal atoms since their atomic orbitals would strongly mix with the molecular orbitals of the cluster anions, complicating the orbital analysis. Instead, at least to partially stabilize the excessive negative charges, we employed the conductor-like screening model (COSMO)[62] with a dielectric constant (ε) of 46.3.[63] This particular value of ε corresponds to the average of the values[64] for ethylene carbonate (ε = 2.8) and diethyl carbonate (ε = 89.8),[65] the two polar solvents used in the experimental MCB setup.[25] In order to analyze the super-reduced POM cluster with the maximum number of Mo triangles, we first examined a *molecular substructure fragment* $[Mo_3O_{13}H_7]^{7-}$ containing a single metal triangle (shown in Figure 7), which was created from structure **9** by saturating edge oxygen atoms with hydrogen atoms where

dx.doi.org/10.1021/ja5032369 | J. Am. Chem. Soc. 2014, 136, 9042−9052

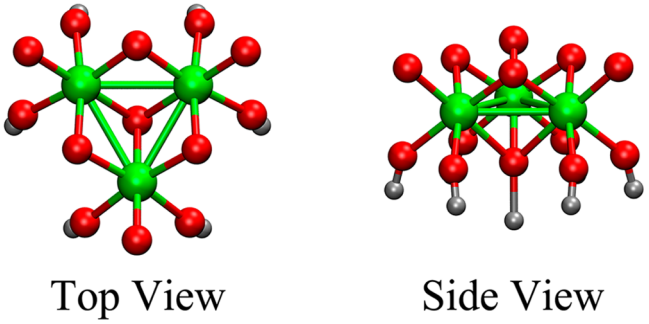

Figure 7. Top and side views of the constructed Mo triangle substructure. The gray spheres indicate hydrogen atoms, and other colors are consistent with the caption of Figure 1.

necessary. Since there are four such substructures in the α-Keggin POM and the super-reduction involves 24 excess electrons, one such substructure formally gains six electrons. The substructure fragment possesses C_{3v} symmetry, and BP86-D/SV(P) calculations including the COSMO dielectric continuum solvation model were performed using this point-group symmetry.

The Kohn–Sham frontier MOs of the $[Mo_3O_{13}H_7]^{7-}$ subunit, shown in Figure 8, indicate that the irreducible representations of the doubly occupied orbitals holding the six additional electrons are e and a_1 (center column of Figure 8). These three MOs arise from hybridization of three Mo 4d orbitals, and the decreased Mo–Mo distances in the Mo triangle enhance the overlap of these orbitals and lower their relative orbital energies. Especially, in the lowest occupied orbital, which contains two excess electrons and has the a_1 irreducible representation, all three Mo atoms interact via a three-center two-electron bonding orbital. The degenerate e MOs correspond to Mo–Mo bonds and simultaneously exhibit a strong antibonding character between Mo atoms participating in the metal–metal bond and the attached outer oxygen atoms, which correspond to the Mo–O (out) bonds of the POM cluster. On the other hand, the LUMO of the reduced substructure possesses antibonding character between the three-center bond and the sp^3 hybrid orbitals on the central oxygen atom. Occupation of this MO by additional excess electrons would result in severe weakening of the cage structure, and thus, a maximum of six excess electrons seems very reasonable for this substructure. As a matter of fact, the existence of triangular metal oxide sites, including the above-described orbital patterns, has been predicted previously by both experiment and theory.[24,66,67] Our MOs here agree quite well with those predicted by Cotton in the 1960s.[66]

In order to extend the MO analysis to the complete POM^{27-} cluster, we used the constructed POM^{27-} structure (Figure 6A) with T_d symmetry. As with the partial substructure MO calculation, the symmetry constraint was used in the BP86-D/SV(P) calculation including the COSMO dielectric continuum solvation method. Once four partial substructures are connected and assembled into POM^{27-}, the four a_1 and eight e frontier MOs containing the excess electrons split into groups of one a_1 + three t_2 MOs and two e + three t_1 + three t_2 MOs, respectively (see the right column of Figure 8). We verified the irreducible representations of the POM^{27-} orbitals and their correspondence to the substructure MOs visually. The LUMO of POM^{27-} is mainly composed of Rydberg 3p orbitals on oxygen atoms (see, e.g., the visualization of the a_1 LUMO of POM^{27-} in Figure 8), indicating that it is impossible to further reduce the α-Keggin POM beyond the addition of 24 electrons.

The Kohn–Sham occupied frontier MOs of the constructed structure can further be analyzed to obtain an even more detailed understanding of the origin of the structural changes of the POM cluster upon super-reduction. In Figure S3 in the SI, five MOs representing the five different irreducible representations of the 12 MOs containing the 24 excess electrons are visualized (only one MO for each degenerate MO level was selected). Three-center orbitals are clearly visible, along with Mo–Mo bonding orbitals. In addition, we found MOs with Mo–O (out) antibonding character. The frontier orbital features are consistent with the existence of Mo triangles and

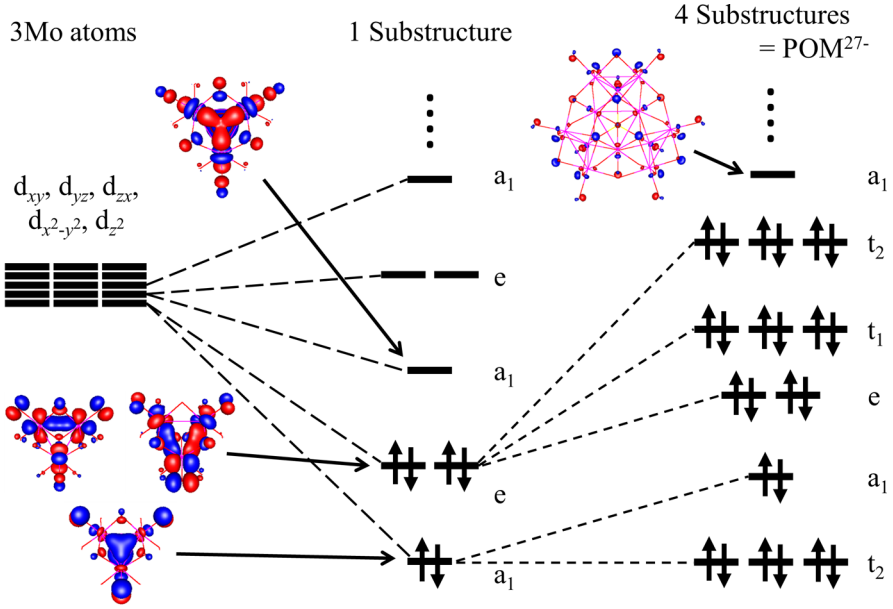

Figure 8. MO diagram for one partial structure (center) and POM^{27-} (right). Arrows indicate excess electrons during reduction (6 and 24 electrons for the partial substructure and POM^{27-}, respectively). The MO isovalue surface corresponds to $\pm 0.05\ (e/a_0)^{1/2}$.

dx.doi.org/10.1021/ja5032369 | J. Am. Chem. Soc. 2014, 136, 9042–9052

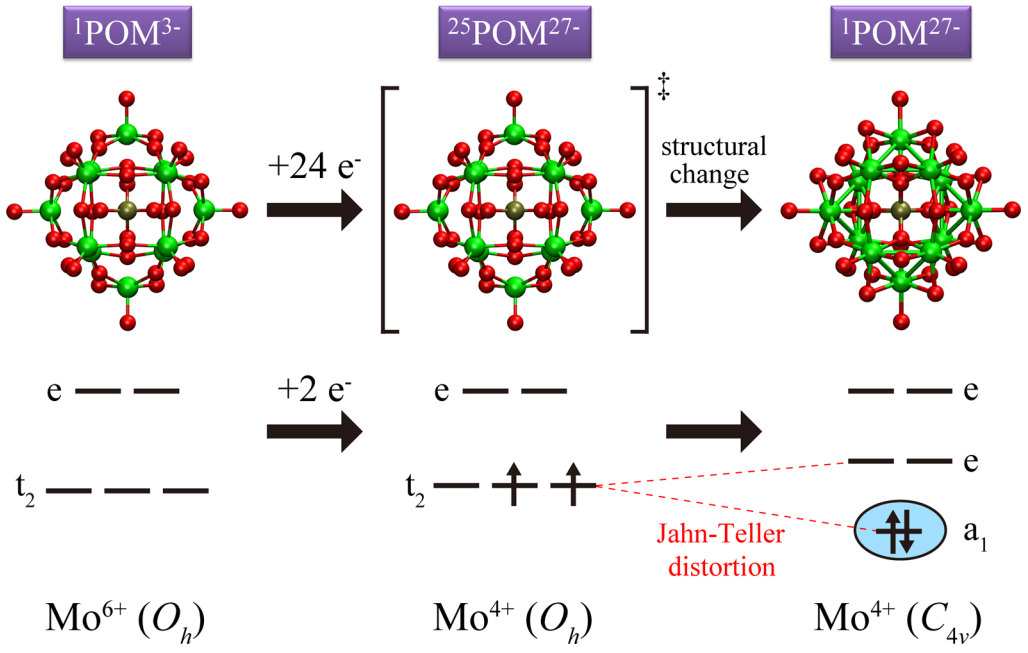

Figure 9. Electronic state change during super-reduction of POM^{3-} by 24 excess electrons. The top panel shows the structures used to compute the $^1POM^{3-}$, $^{25}POM^{27-}$, and $^1POM^{27-}$ geometries, while the bottom panel illustrates the ligand field orbital occupation patterns for a single Mo site coordinated by six oxygen atoms. A Jahn–Teller distortion to a local C_{4v} environment (with the outward-pointing, axial Mo–O bond becoming elongated) lifts the local orbital degeneracy in the doubly occupied t_2 level, resulting in the more stable closed-shell singlet electronic state $^1POM^{27-}$.

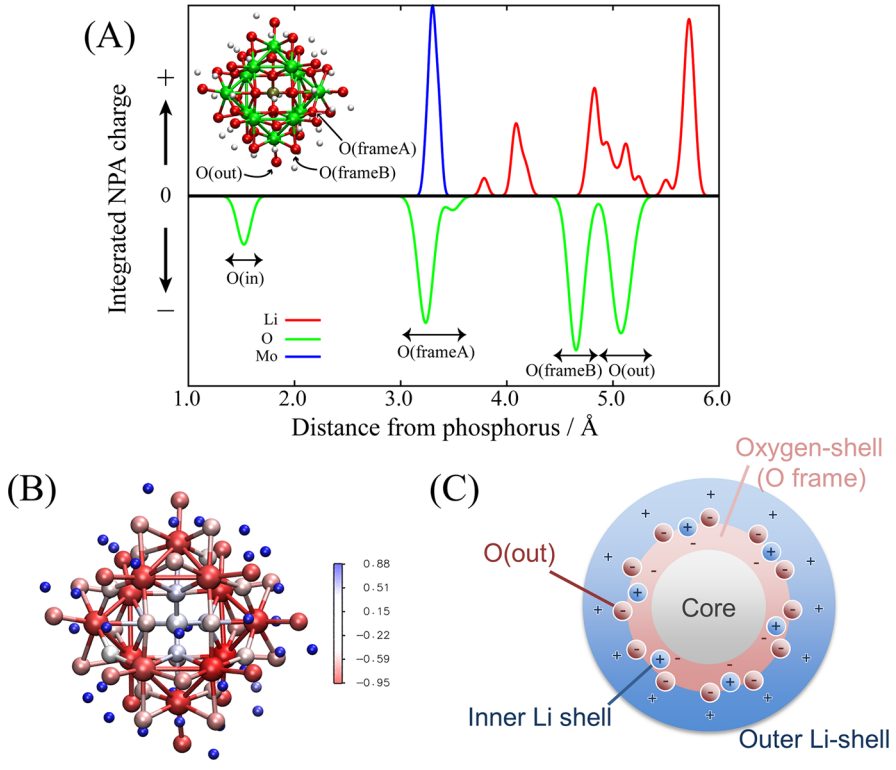

Figure 10. Charge distribution in the constructed and subsequently optimized structure including 35 Li atoms (structure **10** in the SI, depicted in Figure 6B). (A) NPA atomic charges integrated over shells around the phosphorus center. (B) Charge changes during super-reduction of the POM^{3-} cluster by neutral Li atoms. (C) Schematic illustration of the notion of a "semipermeable molecular capacitor".

the elongation of Mo–O (out) bonds observed in the experiment.[25]

All of the calculations described above were performed for closed-shell singlet electronic states. The formal charge of each Mo atom in POM^{3-} is +6, which means that there are no occupied 4d levels on the quasi-octahedrally coordinated Mo atoms (see Figure 9 left). Therefore, the ground state of POM^{3-} is known to be a singlet,[68,69] denoted as $^1POM^{3-}$. However, it is not immediately clear that this is the ground state of the super-reduced POM cluster as well. Thus, we

dx.doi.org/10.1021/ja5032369 | J. Am. Chem. Soc. 2014, 136, 9042–9052

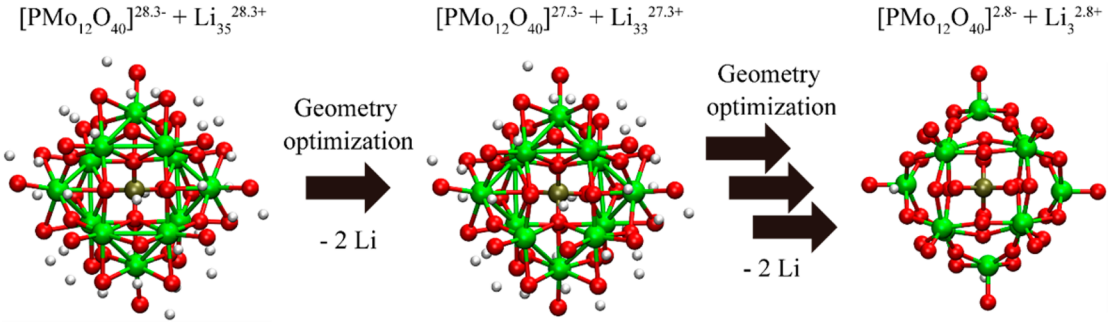

Figure 11. Charging of the super-reduced POM^{27-}. Two Li atoms were removed randomly, and the geometry was reoptimized at the BP86-D/SV(P) level of theory; this procedure was repeated until only three Li atoms remained. The total charge of the system was always set to 0.

computed energy differences between low- and high-spin states at the native X-ray (POM^{3-}, symmetrized to T_d) geometry as well as at the "constructed" (POM^{27-}) T_d geometry. We found that the ground state of POM^{27-} at the POM^{3-} geometry (no Mo−Mo bonds) is actually a state with multiplicity $M = 2S + 1 = 25$ ($^{25}POM^{27-}$) in which all 24 excess electrons carry the same spin. In terms of ligand field theory, in this state two electrons occupy the triply degenerate t_2 atomic 4d levels of each octahedrally coordinated Mo center. The closed-shell singlet $M = 1$ state is 2.63 eV higher in energy. The occupation of the triply degenerate t_2 Mo 4d level (Figure 9 middle) by only two electrons in this geometry triggers a first-order Jahn−Teller effect, reducing the local symmetry of each sixfold-coordinated Mo site from quasi-O_h to quasi-C_{4v}, resulting in largely elongated Mo−O (out) bonds and the formation of Mo−Mo bonds. Correspondingly, the large local Jahn−Teller effects associated with each Mo site hugely stabilize the closed-shell singlet state (Figure 9 right). The gap between closed-shell ground and high-spin $M = 25$ state in the distorted structure is 9.76 eV! The local Jahn−Teller effect is therefore confirmed as the driving force for the molecular and electronic structure changes during super-reduction of the α-Keggin POM cluster.

Super-Reduced POM^{27-} as a Semipermeable Molecular Capacitor. Analysis of the NPA point charges on the atoms of the constructed and subsequently optimized structure including 35 Li atoms (structure **10** in the SI, depicted in Figure 6B) shows that the outer Li shell is strongly positively charged, whereas the oxygen atoms "sticking out" from the POM cluster, namely, O (out) and to a lesser degree O (frameB), are strongly negatively charged. Figure 10A depicts NPA atomic charges integrated over spherical shells around the central phosphorus atom. Roughly speaking, there are three "solvation shells" created by the Li atoms: the innermost layer, which interacts with O (frameA) oxygen atoms; the second solvation shell, which interacts with O (frameB) and O (out) atoms; and the outermost layer, which interacts mostly with O (out) atoms. The second and third solvation shells are close enough to nearly overlap and thus can be classified as a single outer Li shell. The charge−charge interaction between oxygen and Li atoms is difficult to evaluate in this plot because of the presence of the still strongly positively charged, albeit reduced, Mo atoms. Therefore, the changes in the NPA atomic charges upon super-reduction, defined as the differences between the charges in structure **10** and POM^{3-} structure **1**, are shown in Figure 10B. The molecular orientation conforms to that shown in Figure 6B. The electron uptake on Mo is clearly visible (as indicated by the red color) as well as slight and stronger electron uptake on the frame and outward-pointing oxygen atoms, respectively. Li atoms are almost uniformly positively charged, independent of their position. The situation is schematically depicted in Figure 10C, where it becomes clear that interspersion of outer negatively charged oxygen atoms with a large number of positively charged Li atoms in the inner and outer shells clearly plays an important role in overcoming the huge Coulombic repulsive force due to excess charge on the POM cluster by converting it into attractive $Li^{\delta+}-O^{\delta-}$ Coulombic interactions, with Li penetrating deep into the negatively charged outer oxygen layer. Thus, super-reduced POM^{27-} can be viewed as a "semipermeable molecular capacitor" with possible future applications in molecular electronics in addition to its proven effectiveness as a cathode material in MCBs.

Reversibility of the Structural Changes. Thus far we have discussed structural changes during reduction of the cluster ($POM^{3-} \rightarrow POM^{27-}$). In this subsection, we focus on the reverse structural changes for the $POM^{27-} \rightarrow POM^{3-}$ oxidation process, as observed experimentally: even after 10 charge−discharge cycles, the decrease in the battery capacity was insignificant.[25] Therefore, the structural changes during the reduction and oxidation processes must be reversible. To mimic the "oxidation" of the super-reduced POM^{27-} back to POM^{3-}, starting from the neutral "constructed" and optimized structure with 35 Li atoms we removed Li atoms from random positions two at a time and reoptimized the geometries of the resulting structures, again with 0 charge. This procedure was continued until only three Li atoms remained in the system, formally corresponding to POM^{3-}. The procedure is schematically depicted in Figure 11. Indeed, the final structure is very similar to the original BP86-D/SV(P)-optimized POM^{3-} structure **1**. The average discrepancy of bond distances is actually only 0.002 Å, and therefore, we are confident in saying that the reversibility of the reduction and oxidation processes of the POM cluster is supported by theory.

Since our study indicates a clear correlation between the number of excess electrons and the number of Mo−Mo bonds, it was of interest to follow this trend during our artificial oxidation of POM^{27-}. In Figure 12 we have plotted the number of Mo−Mo bonds (i.e., Mo−Mo distances shorter than 3.0 Å) as a function of the NPA-calculated number of excess electrons on the cluster. Interestingly, the number of Mo−Mo bonds is nearly linearly dependent on the number of excess electrons! Our analysis indicates that formation of the first Mo−Mo bond may start around the 12th to 14th excess electron, suggesting that local Jahn−Teller distortions due to partially filled t_2 4d

dx.doi.org/10.1021/ja5032369 | J. Am. Chem. Soc. 2014, 136, 9042−9052

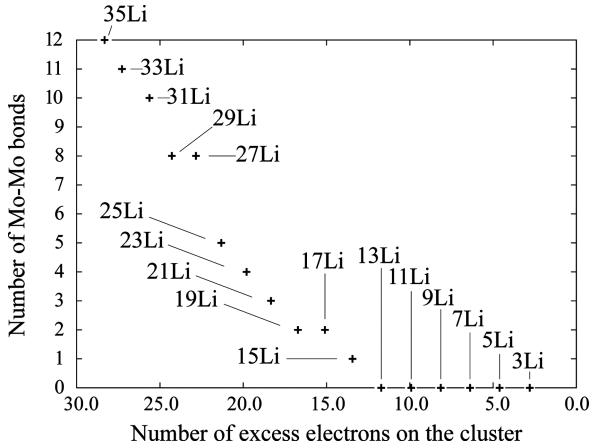

Figure 12. Correlation between the number of excess electrons on the cluster and the number of Mo−Mo bonds (Mo−Mo distances less than 3.0 Å).

levels of *all* Mo atoms of the POM cluster are required for stable metal−metal bond formation.

Design Principles for Improved MCB Cathode Materials. In this work, we have theoretically discussed the structural changes in POMs during discharge in an MCB setup and the origin of their excellent performance via electronic structure analysis. We have noted the importance of metal−metal bonding within the POM cluster and the ability of counterions surrounding it to provide charge compensation. We conclude from our study that in order to design even better MCB cathode materials in the future, the following structural and electronic features need to be present:

(1) a high density of oxygen atoms on the outside of the cluster;
(2) transition-metal atoms with empty degenerate d levels;
(3) geometrical proximity of these metal atoms to allow the formation of metal−metal bonds;
(4) the ability of Li^+ counterions to at least partially migrate into the negatively charged outer oxygen shell to counterbalance the repulsive Coulomb forces due to the presence of excess charges.

In preliminary explorations, we have already carried out analogous calculations on a Dawson POM cluster, $[P_2Mo_{18}O_{62}]^{6-}$, and its super-reduced analogue, $[P_2Mo_{18}O_{62}]^{42-}$. Similar to the α-Keggin POM, we observed the formation of Mo−Mo bonds, but in this case Li atoms migrated into the hollow central site and ripped the cluster apart. Further attempts to design enhanced MCB components are currently ongoing in our laboratories.

SUMMARY

We have theoretically investigated the molecular and electronic structures of the heteropolymolybdate α-Keggin polyoxometalate cluster ($[XMo_{12}O_{40}]^{3-}$, X = P) and its super-reduced state ($[PMo_{12}O_{40}]^{27-}$) as well as those of the tungsten analogues $[PW_{12}O_{40}]^{3-}$ and $[PW_{12}O_{40}]^{27-}$. DFT geometry optimizations and FPMD simulations of neutral aggregate species with explicit inclusion of Li atoms around the POM cluster as counterions showed that metal−metal bonds and triangular metal sites are formed as a result of increasing uptake of excess electrons on the molecular cage. The formation of Mo−Mo bonds during discharge in an MCB is in agreement with previous EXAFS structural data.[25] At that time, elongation of Mo−O bonds was also observed, which we attribute to the conversion of Mo═O double bonds pointing out from the individual Mo octahedra to Mo−O single bonds, where the oxygen atom becomes negatively charged and favorably interacts with the surrounding Li^+ countercations. At the same time, during the formation of the Mo triangles, O (frameB) atoms bridging the participant Mo atoms become "squeezed out" and form another attraction point for favorable interactions with the Li^+ countercations, which were found to form an inner and an outer shell around the POM cluster. The interspersion of positive and negative charges on the outside of the cluster core contributes to overcoming the huge repulsive Coulombic forces due to the presence of 27 negative charges on the POM. *The super-reduced POM can be viewed as a "semiporous molecular capacitor" with possibly broader applications in molecular electronics.*

Electronic structure analysis of a "constructed" structure with T_d symmetry that possesses the maximum number of four Mo triangles in the α-Keggin POM was carried out in order to understand the origin of the structural changes during super-reduction. The existence of a three-center two-electron bond at the center of each triangular Mo site was confirmed, and it was found that Mo−Mo bonds are strongly mixed with Mo−O antibonds, shuffling electrons partially away from the Mo sites to the increasingly negatively charged oxygen atoms, which then favorably interact with Li^+ countercations. The driving force for the formation of Mo−Mo bonds was found to be a local Jahn−Teller distortion at individual Mo octahedral sites, where the triply degenerate t_2 4d orbitals become partially filled during reduction.

Finally, we verified that the reversible structural change of oxidation is plausible theoretically, and the results indirectly indicate that Mo−Mo bond formation is a stepwise process. Our calculation implies that the first Mo−Mo bond formation may occur after reduction by 12 to 14 electrons. Calculations on the W analogues indicate that the same molecular and electronic structure changes in W-POM can be expected, but because of the heavier mass of W in comparison to Mo, its capacity in MCBs is expected to be much smaller. From the above findings, we have derived design principles for future improved MCB cathode materials based on POMs.

ASSOCIATED CONTENT

Supporting Information

Results of FPMD simulations of super-reduced POM with sodium atoms and Cartesian coordinates of optimized structures as indicated in the text. This material is available free of charge via the Internet at http://pubs.acs.org.

AUTHOR INFORMATION

Corresponding Author

sirle@chem.nagoya-u.ac.jp

Notes

The authors declare no competing financial interest.

ACKNOWLEDGMENTS

We thank Prof. Josep Poblet and Mr. Pablo Aparicio (Rovira i Virgili University), Dr. Klavs Hansen (University of Gothenburg), and Craig Fisher (Japan Fine Ceramics Center) for helpful discussions. Computations were partially performed at the Research Center for Computational Science of the Institute for Molecular Science (IMS) in Okazaki, Japan. Y.N. was

supported by a Research Fellowship for Young Scientists (DC1) from the Japan Society for the Promotion of Science (JSPS). This work was partially supported by the MEXT Project of Integrated Research on Chemical Synthesis.

REFERENCES

(1) Hill, C. L. *Chem. Rev.* **1998**, *98*, 1−2.
(2) Gouzerh, P.; Che, M. *Actual. Chim.* **2006**, No. 298, 9−22.
(3) Keggin, J. F. *Nature* **1933**, *131*, 908−909.
(4) Lindqvist, I. *Acta Crystallogr.* **1950**, *3*, 159−160.
(5) Evans, H. T., Jr. *J. Am. Chem. Soc.* **1948**, *70*, 1291−1292.
(6) Anderson, J. S. *Nature* **1937**, *140*, 850.
(7) Dawson, B. *Acta Crystallogr.* **1953**, *6*, 113−126.
(8) López, X.; Miró, P.; Carbó, J. J.; Rodríguez-Fortea, A.; Bo, C.; Poblet, J. M. *Theor. Chem. Acc.* **2011**, *128*, 393−404.
(9) Neumann, R.; Dahan, M. *Nature* **1997**, *388*, 353−355.
(10) Sartorel, A.; Carraro, M.; Scorrano, G.; Zorzi, R. D.; Geremia, S.; McDaniel, N. D.; Bernhard, S.; Bonchio, M. *J. Am. Chem. Soc.* **2008**, *130*, 5006−5007.
(11) Compain, J.-D.; Mialane, P.; Dolbecq, A.; Mbomekallé, I. M.; Marrot, J.; Sécheresse, F.; Riviére, E.; Rogez, G.; Wernsdorfer, W. *Angew. Chem.* **2009**, *121*, 3123−3127.
(12) Chiang, M.-H.; Dzielawa, J. A.; Dietz, M. L.; Antonio, M. R. *J. Electroanal. Chem.* **2004**, *567*, 77−84.
(13) Volkmer, D.; Bredenköker, B.; Kögerler, P.; Kurth, D. G.; Lehmann, P.; Schnablegger, H.; Schwahn, D.; Pipenbrink, M.; Krebs, B. *J. Am. Chem. Soc.* **2002**, *124*, 10489−10496.
(14) Bagno, A.; Bonchio, M. *Angew. Chem.* **2005**, *117*, 2059−2062.
(15) Rodríguez-Fortea, A.; de Graaf, C.; Poblet, J. M. *Chem. Phys. Lett.* **2006**, *428*, 88−92.
(16) Macht, J.; Janik, M. J.; Neurock, M.; Iglesia, E. *Angew. Chem.* **2007**, *119*, 8010−8014.
(17) Yan, L.; López, X.; Carbó, J. J.; Sniatynsky, R.; Duncan, D. C.; Poblet, J. M. *J. Am. Chem. Soc.* **2008**, *130*, 8223−8233.
(18) Aparicio, P. A.; Poblet, J. M.; López, X. *Eur. J. Inorg. Chem.* **2013**, 1910−1916.
(19) Lira-Cantú, M.; Gómez-Romero, P. *Chem. Mater.* **1998**, *10*, 698−704.
(20) Azumi, B. M.; Ishihara, T.; Nishiguchi, H.; Takita, Y. *Electrochemistry* **2002**, *70*, 869−874.
(21) Pope, M. T.; Müller, A. *Angew. Chem., Int. Ed. Engl.* **1991**, *30*, 34−38.
(22) Kuznetsov, A. E.; Geletii, Y. V.; Hill, C. L.; Morokuma, K.; Musaev, D. G. *J. Am. Chem. Soc.* **2009**, *131*, 6844−6854.
(23) Kawasaki, N.; Wang, H.; Nakanishi, R.; Hamanaka, S.; Kitaura, R.; Shinohara, H.; Yokoyama, T.; Yoshikawa, H.; Awaga, K. *Angew. Chem., Int. Ed.* **2011**, *123*, 3533−3536.
(24) Launay, J. P. *J. Inorg. Nucl. Chem.* **1976**, *38*, 807−816.
(25) Wang, H.; Hamanaka, S.; Nishimoto, Y.; Irle, S.; Yokoyama, T.; Yoshikawa, H.; Awaga, K. *J. Am. Chem. Soc.* **2012**, *134*, 4918−4924.
(26) Yoshikawa, H.; Hamanaka, S.; Miyoshi, Y.; Kondo, Y.; Shigematsu, S.; Akutagawa, N.; Sato, M.; Yokoyama, T.; Awaga, K. *Inorg. Chem.* **2009**, *48*, 9057−9059.
(27) Wang, H.; Hamanaka, S.; Yokoyama, T.; Yoshikawa, H.; Awaga, K. *Chem.—Asian J.* **2011**, *6*, 1074−1079.
(28) Heering, H. A.; Bulsink, Y. B. M.; Hagen, W. R.; Meyer, T. E. *Eur. J. Biochem.* **1995**, *232*, 811−817.
(29) Torres, R. A.; Loveil, T.; Noodleman, L.; Case, D. A. *J. Am. Chem. Soc.* **2003**, *125*, 1923−1936.
(30) Liu, S.; Wang, C.; Zhai, H.; Li, D. *J. Mol. Struct.* **2003**, *654*, 215−221.
(31) Atkins, P.; Friedman, R. *Molecular Quantum Mechanics*; Oxford University Press: New York, 2005; pp 122−167.
(32) Hohenberg, P.; Kohn, W. *Phys. Rev.* **1964**, *136*, B864−B871.
(33) Kohn, W.; Sham, L. J. *Phys. Rev.* **1965**, *140*, A1133−A1138.
(34) TURBOMOLE V6.2 2010, a development of University of Karlsruhe and Forschungszentrum Karlsruhe GmbH, 1989−2007, TURBOMOLE GmbH since 2007; available from http://www.turbomole.com.
(35) Becke, A. D. *Phys. Rev. A* **1988**, *38*, 3098−3100.
(36) Perdew, J. P. *Phys. Rev. B* **1986**, *33*, 8822−8824.
(37) Becke, A. D. *J. Chem. Phys.* **1993**, *98*, 5648−5652.
(38) Schäfer, A.; Horn, H.; Ahlrichs, R. *J. Chem. Phys.* **1992**, *97*, 2571−2577.
(39) Eichkorn, K.; Weigend, F.; Treutler, O.; Ahlrichs, R. *Theor. Chem. Acc.* **1997**, *97*, 119−124.
(40) Weigend, F.; Häser, M.; Patzelt, H.; Ahlrichs, R. *Chem. Phys. Lett.* **1998**, *294*, 143−152.
(41) Eichkorn, K.; Treutler, O.; Öhm, H.; Häser, M.; Ahlrichs, R. *Chem. Phys. Lett.* **1995**, *240*, 652−660.
(42) Weigend, F. *Phys. Chem. Chem. Phys.* **2006**, *8*, 1057−1065.
(43) Grimme, S. *J. Comput. Chem.* **2006**, *27*, 1787−1799.
(44) Nose, S. *J. Chem. Phys.* **1984**, *81*, 511−519.
(45) Hoover, W. G. *Phys. Rev. A* **1985**, *31*, 1695−1697.
(46) Martyna, G. J.; Klein, M. L.; Tuckerman, M. *J. Chem. Phys.* **1992**, *97*, 2634−2643.
(47) Gorelsky, S. I. *AOMix: Program for Molecular Orbital Analysis*; University of Ottawa: Ottawa, ON, 2011; available at http://www.sg-chem.net/.
(48) Gorelsky, S. I.; Lever, A. B. P. *J. Organomet. Chem.* **2001**, *635*, 187−196.
(49) Reed, A. B.; Weinstock, R. B.; Weinhold, F. *J. Chem. Phys.* **1985**, *83*, 735−746.
(50) Wiberg, K. B. *Tetrahedron* **1968**, *24*, 1083−1096.
(51) Humphrey, W.; Dalke, A.; Schulten, K. *J. Mol. Graphics* **1996**, *14*, 33−38.
(52) Laaksonen, L. *J. Mol. Graphics* **1992**, *10*, 33−34.
(53) Bergman, D. L.; Laaksonen, L.; Laaksonen, A. *J. Mol. Graphics Modell.* **1997**, *15*, 301−306.
(54) Koch, W.; Holthausen, M. C. *A Chemist's Guide to Density Functional Theory*, 2nd ed.; Wiley-VCH: Weinheim, Germany, 2001; pp 119−136.
(55) Minenkov, Y.; Singstad, A.; Occhipinti, G.; Jensen, V. R. *Dalton Trans.* **2012**, *41*, 5526−5541.
(56) Simons, J. *Molecular Anions* (Web-based textbook); http://www.hec.utah.edu/anions/Molecular%20Anions.pdf.
(57) Møller, C.; Plesset, M. S. *Phys. Rev.* **1934**, *46*, 618−622.
(58) Szabo, A.; Ostlund, N. S. *Modern Quantum Chemistry*; Dover Publications: New York, 1996; pp 231−270.
(59) Fleming, C.; Long, D.-L.; McMillan, N.; Johnston, J.; Bovet, N.; Dhanak, V.; Gadegaard, N.; Kögerler, P.; Cronin, L.; Kadodwala, M. *Nat. Nanotechnol.* **2008**, *3*, 229−233.
(60) Slater, J. C. *J. Chem. Phys.* **1964**, *41*, 3199−3204.
(61) Hayaki, S.; Kido, K.; Yokogawa, D.; Sato, H.; Sakaki, S. *J. Phys. Chem. B* **2009**, *113*, 8227−8230.
(62) Klamt, A.; Schüürmann, G. *J. Chem. Soc., Perkin Trans. 2* **1993**, *5*, 799−805.
(63) The conductor-like screening model (COSMO) solvation model was also tested instead of using countercations, but the dielectric continuum-type solvation model cannot stabilize surplus electrons sufficiently and during self-consistent-field cycles failed to converge after several geometry optimization cycles.
(64) *CRC Handbook of Chemistry and Physics*, 89th ed. (CD-ROM version 2009); Lide, D. R., Ed.; CRC Press: Boca Raton, FL, 2009.
(65) Using the average of two dielectric constants was only a compromise since we had no other means to treat the solvent structure of the mixture of two solvents in more sophisticated ways.
(66) Cotton, F. A. *Inorg. Chem.* **1964**, *3*, 1217−1220.
(67) Ansell, G. B.; Katz, L. *Acta Crystallogr.* **1966**, *21*, 482−485.
(68) Le Magueres, P.; Ouahab, L.; Golhen, S.; Grandjean, D.; Pena, O.; Jegaden, J.-C.; Gomez-Garcia, C. J.; Delaes, P. *Inorg. Chem.* **1994**, *33*, 5180−5187.
(69) Poblet, J. M.; López, X.; Bo, C. *Chem. Soc. Rev.* **2003**, *32*, 297−308.